[Supplementary Information]

Acoustic energy harvesting meta-surface by coupling nonlinear Helmholtz resonator and auxetic structure

Xinzong Wang[a], Xiao Guo[a], Xinghao Hu[a], Shengkang Zong[a], Jiao Shen[a], Xiaofang Kang[c], Shaojie Ma[c], Haiyan Fan[a,b], Yifan Zhu[a,b*], Hui Zhang[a,b*]

[a] Jiangsu Key Laboratory for Design and Manufacturing of Precision Medicine Equipment, School of Mechanical Engineering, Southeast University, Nanjing 211189, China

[b] Key Laboratory of Underwater Acoustic Signal Processing (Southeast University), Ministry of Education, Nanjing, 210096, China

[c] School of Civil Engineering, Anhui Jianzhu University, Hefei 230601, China

*Correspondence to: yifanzhu@seu.edu.cn (Y. Zhu) and seuzhanghui@seu.edu.cn (H. Zhang)

Contents

S1 Melnikov theoretical analysis

According to Eq. (7) in the main text, the potential energy function of the system is:

$$E_P(x) = \frac{1}{2}x^2 - \frac{1}{3}\alpha x^3 + \frac{1}{4}\beta x^4 \tag{S1}$$

The application of the Melnikov method necessitates the transformation of Eq. (7) into an equivalent system of first-order ordinary differential equations:

$$y = \dot{x} \tag{S2}$$

$$\dot{y} = -x + \alpha x^2 - \beta x^3 + F\cos(\omega\tau) - \zeta\dot{x} \tag{S3}$$

Under small perturbations, the system is regarded as a Hamiltonian system:

$$y = \dot{x} \tag{S4}$$

$$\dot{y} = -x + \alpha x^2 - \beta x^3 + \varepsilon(\tilde{F}\cos(\omega\tau) - \tilde{\zeta}\dot{x}) \tag{S5}$$

where $\tilde{F} = F/\varepsilon$, $\tilde{\zeta} = \zeta/\varepsilon$, ε is a small perturbed factor [1,2].

When $\varepsilon = 0$, the corresponding unperturbed Hamiltonian system is:

$$y = \dot{x} \tag{S6}$$

$$\dot{y} = -x + \alpha x^2 - \beta x^3 \tag{S7}$$

Substituting $\dot{y} = y = \dot{x} = 0$ into Eqs. (S6) and (S7) yields three fixed points:

$$\text{O } (0, 0) \tag{S8}$$

$$\text{A } \left(\frac{\alpha - \sqrt{\alpha^2 - 4\beta}}{2\beta}, 0\right) \tag{S9}$$

$$\mathrm{B}\left(\frac{\alpha+\sqrt{\alpha^2-4\beta}}{2\beta}, 0\right) \tag{S10}$$

Point O and point B are the centers, and point A is the saddle point. At this point, the system's Hamilton equations take the form of the sum of kinetic and potential energy:

$$H(x, y)=\frac{1}{2}y^2+\frac{1}{2}x^2-\frac{1}{3}\alpha x^3+\frac{1}{4}\beta x^4 \tag{S11}$$

The parametric equation of the homoclinic trajectories is:

$$x_i(\tau)=\pm\frac{2\sqrt{2}\alpha}{3\beta}\frac{\exp\left(\pm\frac{\alpha}{3\sqrt{\beta}}\tau\right)}{\exp\left(\pm\frac{2\alpha}{3\sqrt{\beta}}\tau\right)+1}-\frac{\alpha}{3\beta} \tag{S12}$$

$$y_i(\tau)=\pm\frac{2\sqrt{2}\alpha^2}{9\beta^2\sqrt{\beta}}\frac{1-\exp\left(\pm\frac{2\alpha}{3\sqrt{\beta}}\tau\right)}{\left[\exp\left(\pm\frac{2\alpha}{3\sqrt{\beta}}\tau\right)+1\right]^2} \tag{S13}$$

where $i=1, 2$.

Definition of the Melnikov function for perturbed system:

$$M_i(s)=-\zeta\int_{-\infty}^{+\infty}\left[y_i(\tau)\right]^2 d\tau+F\int_{-\infty}^{+\infty}y_i(\tau)cos[\omega(\tau+s)]d\tau \tag{S14}$$

Subsequently, by Melnikov method, let $M_i(s)=0$

$$sin(\omega s) = \frac{\frac{4}{81}\tilde{\zeta}\left[\left(\frac{\alpha^2}{\beta^3}\right)^{1.5} - \left(\frac{\alpha}{\beta}\right)^3\left(\frac{1}{\beta} - 1\right)^{1.5}\right]}{2\sqrt{2}\tilde{F}\omega\pi\exp\left(\frac{3\omega\pi\sqrt{\beta}}{\alpha}\right)}[ch(\frac{3\omega\pi\sqrt{\beta}}{\alpha}) + 1]\sqrt{\beta} \quad \text{(S15)}$$

To ensure $sin(\omega s) < 1$,

$$F > \frac{2\zeta\left[\left(\frac{\alpha^2}{\beta^3}\right)^{1.5} - \left(\frac{\alpha}{\beta}\right)^3\left(\frac{1}{\beta} - 1\right)^{1.5}\right]}{81\sqrt{2}\omega\pi\exp\left(\frac{3\omega\pi\sqrt{\beta}}{\alpha}\right)}[ch(\frac{3\omega\pi\sqrt{\beta}}{\alpha}) + 1]\sqrt{\beta} \quad \text{(S16)}$$

S2 Identification of coexisting solutions

Nonlinear dynamical systems are characterized by the potential for multiple coexisting attractors, each associated with a specific basin of attraction. The numerical study of these solutions requires an analysis of steady-state trajectories from diverse initial conditions in the phase plane. This work examines the resulting basin structure, as its distribution is critical for understanding system behavior. A fundamental question in both theory and application is determining the final asymptotic state reached from a given initial condition.

This section contains information about the system's coexisting basins of attraction and the information within the basins of attraction. Fig. S1 illustrates the distribution of basins of attraction under different parameter values (corresponding to different steady states). The steady-state trajectories within each basin of attraction can be referenced in Fig. S2, while the proportion of area occupied by each basin of attraction is detailed in Table S1.

Within the specified phase plane range, numerical tests were conducted on the coexisting solutions of the system. As shown in Fig. S1, the basins of attraction were plotted for model

analysis. The fundamental information within each basin of attraction is presented in Table S1 and Fig. S2. To estimate the occurrence probability A of each basin, we calculated the ratio of initial conditions encompassed by the respective basin in Fig. S1. This color-coding is consistently applied in Table S1 and Fig. S1.

When the HR system is in a bi-stable state (Fig. S1(a-c)), coexisting solutions manifest as inter-well oscillations and intra-well oscillations. The depth and width of the potential well significantly influence the basin of attraction corresponding to intra-well oscillations. Compared to shallow and narrow wells, deeper and wider wells are more likely to harbour trajectories within their potential wells. When the HR system is in a mono-stable state, its potential energy function contains only a single potential well (Fig. S1(d-f) and Fig. S1(g-i)). Therefore, regardless of the excitation frequency band, the system oscillates exclusively within this unique potential well. The choice of initial conditions alters the energy of the system's trajectory. The entire basin of attraction manifests as a vortex. The fractal boundary becomes more pronounced near the vortex center, while it begins to blur as one moves away from the vortex core. The structure of the basin of attraction readily forms irregular regions characterized by intense mixing.

Table S1. Values of the system's parameters in a mathematical sense.

Object	Parameter values			*Solution – I*	*Solution – II*	*Solution – III*	*Solution – IV*
	α	β	ω				
Fig. 4(a)	1.2	0.2	0.9	A=33.2%	A=66.8%	—	—
Fig. 4(b)	1.2	0.2	1.1	A=47.6%	—	A=52.4%	—
Fig. 4(c)	1.2	0.2	1.5	A=58.8%	A=13.7%	A=27.5%	—
Fig. 4(d)	1.2	0.4	2.1	A=19.2%	A=80.8%	—	—
Fig. 4(e)	1.2	0.4	2.2	A=71.3%	A=7.3%	A=21.4%	—

Fig. 4(f)	1.2	0.4	2.4	A=10%	A=61.5%	A=23.3%	A=5.2%
Fig. 4(g)	1.2	1.36	1.55	A=28%	A=29.9%	A=42.1%	—
Fig. 4(h)	1.2	1.36	1.65	A=34.6%	A=57.8%	A=7.6%	—
Fig. 4(i)	1.2	1.36	1.75	A=13.8%	A=86%	A=0.2%	—

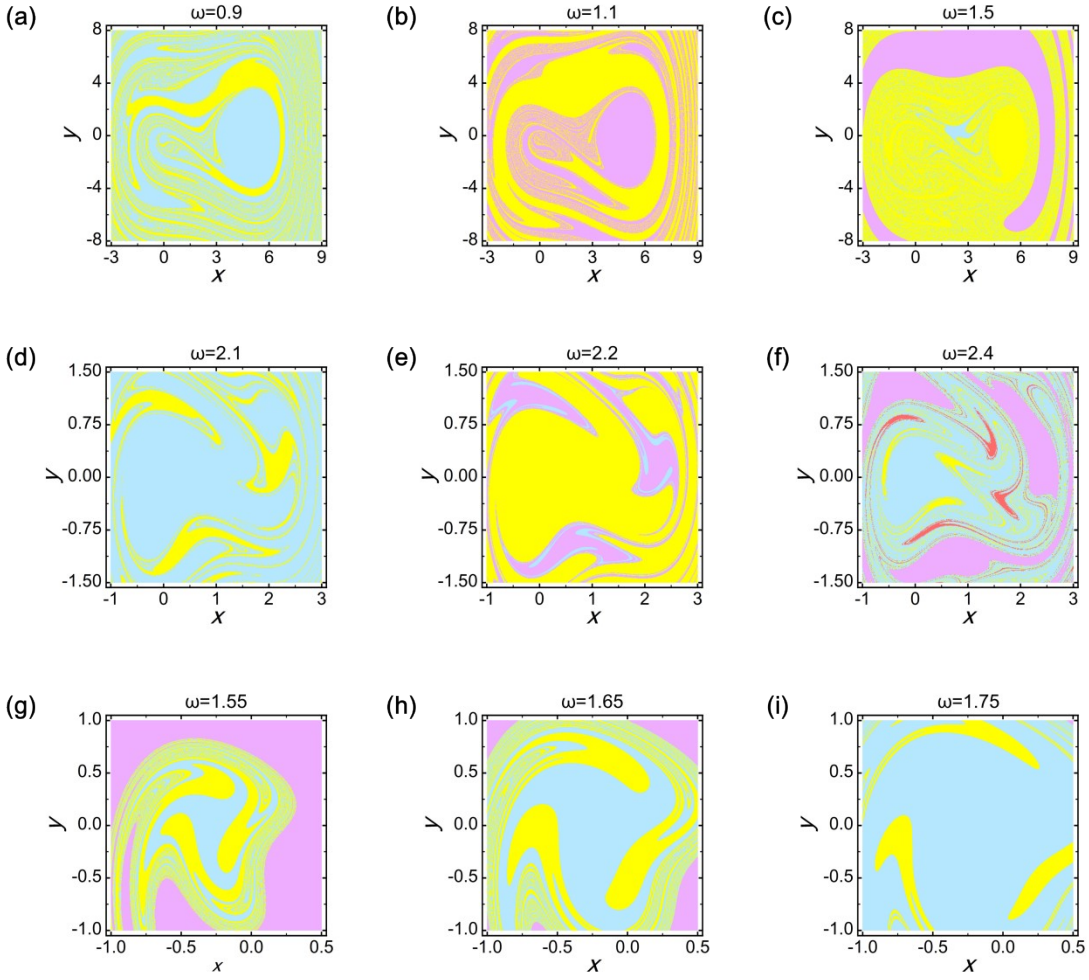

Fig. S1. The distribution of basins of attraction, along with the internal information and parameter values of the basins of attraction, can be referenced in Table S1. (a-c) Asymmetric bi-stable state. (d-f) Quasi-zero stiffness state. (g-i) Mono-stable state.

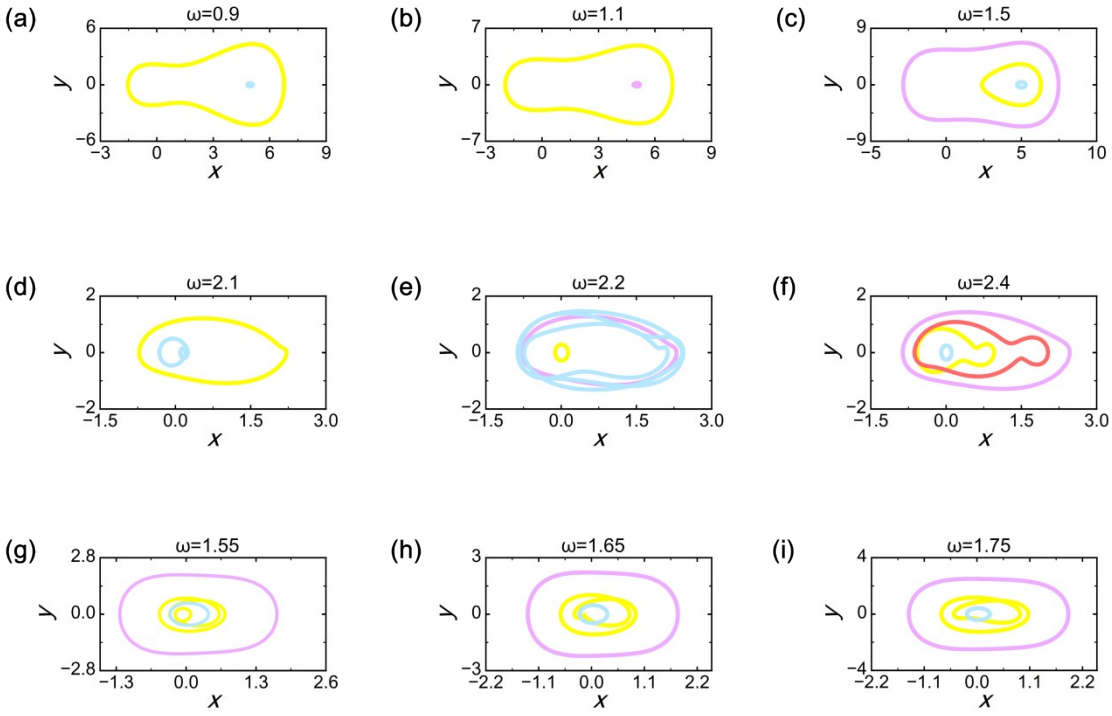

Fig. S2. The phase trajectory curves of the system in each color region are given in terms of the distribution of basins of attraction shown in Fig. S1.

S3 Results and analysis

An AEHMS finite element model was established in COMSOL Multiphysics software, with its geometric and physical parameters as shown in Table S2.

Fig. S3 demonstrates the variation in sound pressure amplitude within the HR as the height H_1 of the noise input module and the diameter R_1 of the circle change, for pillar heights H_s of 0.015 m, 0.025 m, and 0.035 m. Each color-coded area indicates the magnitude of sound pressure amplitude. As the radius of the circle decreases, the HR exhibits a high degree of sensitivity to noise input modules. The height of the pillar primarily affects the volume V_c of the HR, which in turn influences the resonance frequency of the HR.

Table S2. Model parameters for experimental testing and numerical simulation.

Parameter description	Symbol	Parameter values
Helmholtz resonator (ABS)		
Density		1050kg/m^3
Poisson's ratio		0.35
Young's modulus		2.49 × 10^{9}Pa
Height of the HR	h_c	60mm
Length of the square side of the HR base plate	L_c	170mm
Thickness of the side walls and bottom plate of the HR cavity	t_1	15mm
Radius of the neck	R_n	20mm
Length of the neck	L_n	30mm
Noise input module (ABS)		
Radius of the frustum of a cone cavity	R_1	120mm
	R_2	26mm
Side length of the rectangular prism	L_1	250mm
Height of the noise input module	H_1	50mm
Piezoelectric element (PZT-5H)		
Density		7600kg/m^3
Length of the piezoelectric element		24mm
Width of the piezoelectric element		16mm
Thickness of the piezoelectric element		0.3mm
Piezoelectric beam (Aluminium)		
Density		2750kg/m^3
Poisson's ratio		7 × 10^{10}Pa

Young's modulus		0.33
Thickness of the piezoelectric beam	t_2	2mm
Length of the piezoelectric beam	L	73mm
Width of the piezoelectric beam	d	16mm
Geometric parameters of auxetic structure	h_1	24mm
	h_2	8mm
	d_1	2mm
	d_2	2mm
	d_3	2mm
	d_4	2mm
	w_1	1mm
	w_2	16mm

The specific arrangement of the experimental equipment is shown in Fig. S4. A single acoustic barrier unit was employed to simulate the behavior of the entire assembly. The prepared test unit comprised a piezoelectric beam whose base was fixed to the foundation. The base plate is assembled with the HR unit. Sound field control is achieved through a computer control system, which drives the speakers via commands. The voltage output signal from the piezoelectric beam is displayed on an oscilloscope and recorded by the computer.

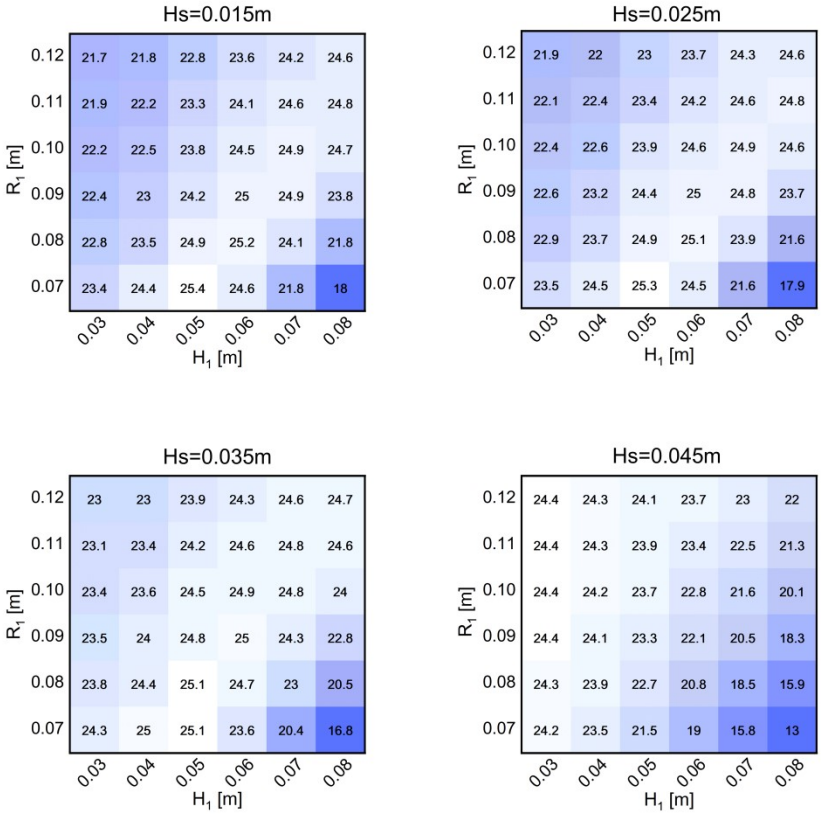

Fig. S3. The effect of parameter variations in noise input modules on sound pressure gain.

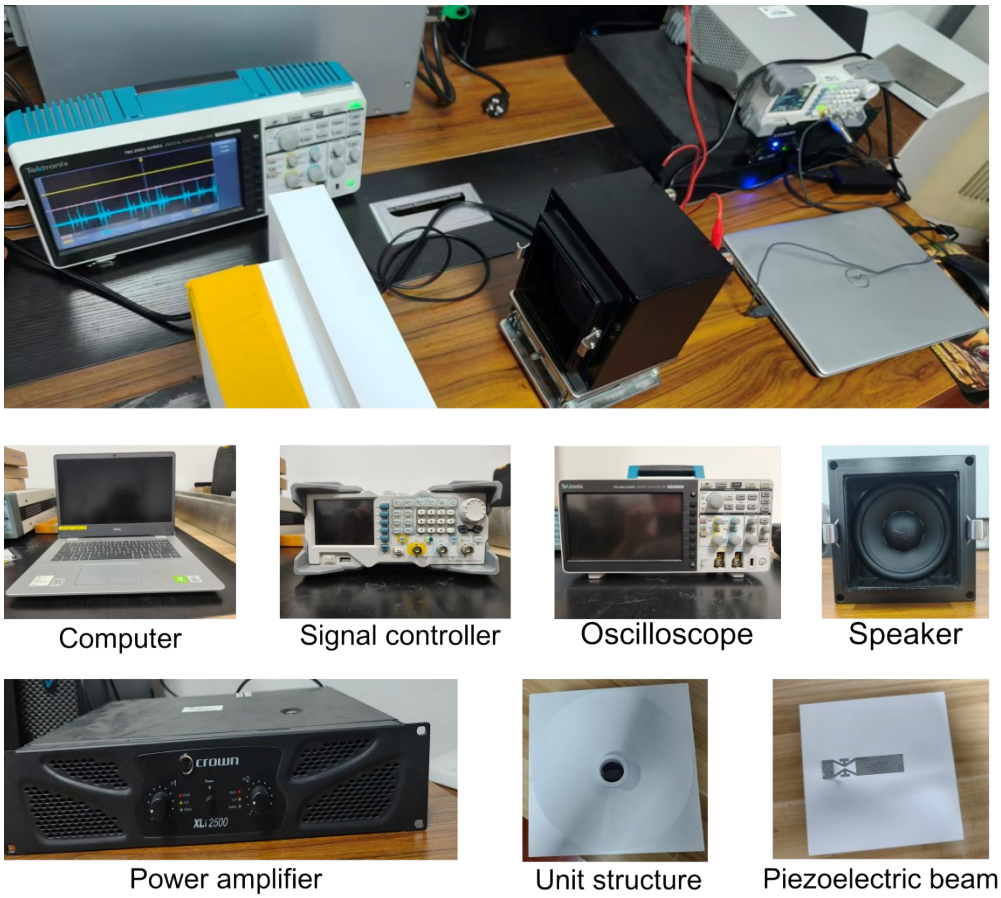

Fig. S4. Introduction to AEHMS and experimental equipment.

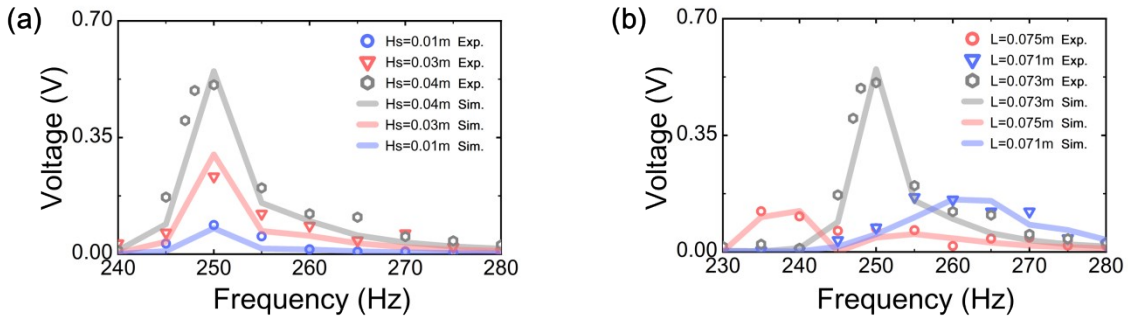

Fig. S5. The Influence of parameters H_s and L on the energy harvesting performance of AEHMS.

Fig. S5 shows the amplitude-frequency response curves of the induced voltage of AEHMS. This study investigates the height H_s of the pillar and the length L of the beam. Parameter L affects the beam's stiffness and resonant frequency. Adjusting parameter L enables acoustic resonance matching between the beam and the cavity.

Table S3. Selection of physical parameters for HR devices under strong stimulation.

Parameter description	Symbol	Parameter values
Helmholtz resonator (ABS)		
Density		1050kg/m^3
Poisson's ratio		0.35
Young's modulus		2.49 × 10^{9}Pa
Height of the HR	h_c	21.5mm
Length of the square side of the HR base plate	L_c	45mm
External radius of the neck	R_E	4mm
Internal radius of the neck	R_I	2mm
Length of the neck	L_n	9mm

To further investigate the nonlinear fluctuations in sound pressure within the Helmholtz resonator cavity, the resonator was scaled down (increasing the likelihood that air particles in the resonator′s neck would enter a nonlinear state). The parameter settings for the Helmholtz resonator are taken from Table S3. R_E is the outer radius of the neck, while R_I is the inner radius of the neck.

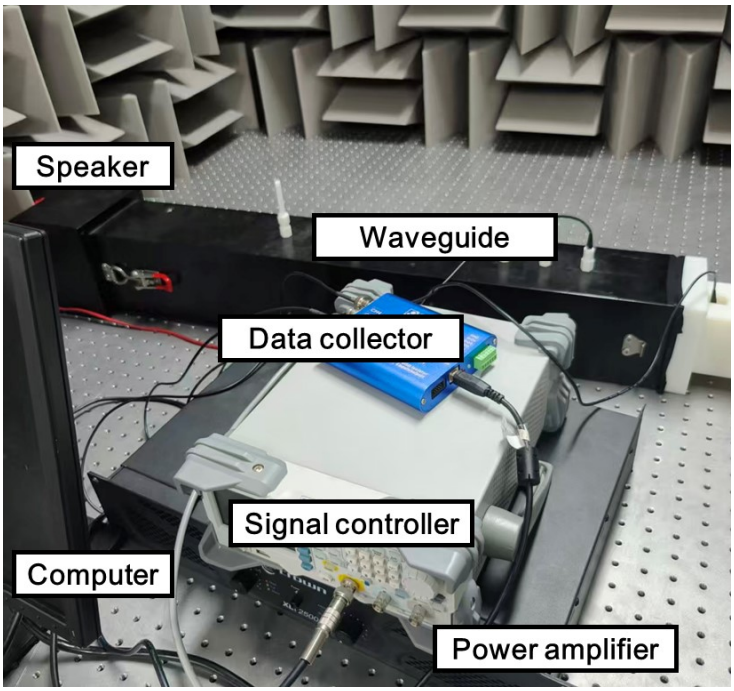

Fig. S6. The experimental setup for acoustic nonlinearity testing.

Fig. S6 shows the experimental setup for testing the nonlinearity of sound pressure fluctuations inside a Helmholtz resonator. The dimensions of the Helmholtz resonator are listed in Table S3. In the experiment (Fig. 6), a sound pressure amplitude of 22 Pa already constitutes a very high external excitation; even with this high-intensity excitation, only slight nonlinear fluctuations in the sound pressure can be observed. Given our current experimental setup, it is extremely difficult to induce a chaotic state in the sound pressure within the Helmholtz resonator [3]. Therefore, to further investigate the sound pressure fluctuations within the Helmholtz resonator cavity, we conducted a simulation analysis, as shown in Fig. S7. In the figure, the horizontal axis represents time, and the vertical axis A represents the ratio of the sound pressure inside the cavity to the input sound pressure. The dimensionless parameter F for the excitation amplitude is 7.

Under the influence of a stronger acoustic excitation, the resonance frequency of the sound pressure fluctuations within the HR changed significantly (from the original 272 Hz to 805 Hz).

By selecting two frequency points in the chaotic state far from the region of maximum resonance for observation, we can see that even far from the region of maximum resonance, the sound pressure fluctuations in the chaotic state still exhibit significant amplitude. In contrast, the frequency point on the left (816 Hz), which is very close to the maximum resonance frequency, exhibits a single-cycle state, with a much smaller amplitude of oscillation compared to the other frequency points. This indicates that nonlinear systems can overcome frequency limitations under chaotic, bifurcated, and threshold conditions, thereby enabling efficient energy conversion across a broader range of environmental vibrations.

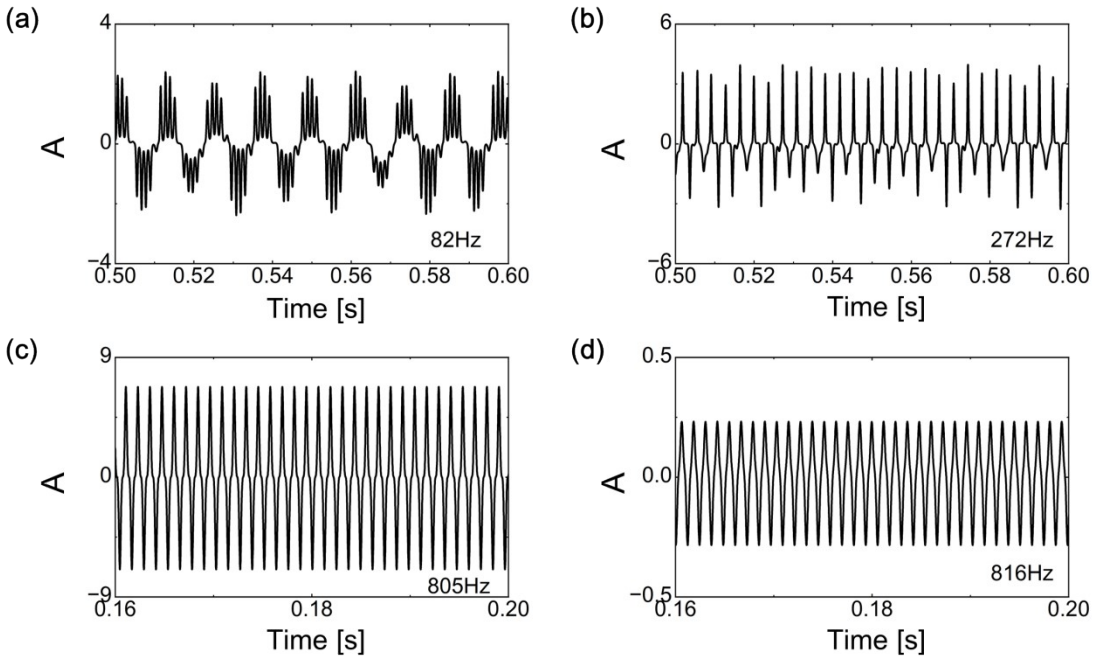

Fig. S7. Under strong excitation, nonlinear fluctuations in sound pressure generated by the HR cavity.

Fig. S8 shows a meta-surface acoustic barrier, which we have divided into nine regions and labeled. The relationship between the output voltage and the excitation frequency for the nine regions of the meta-surface acoustic barrier is shown in Fig. S9.

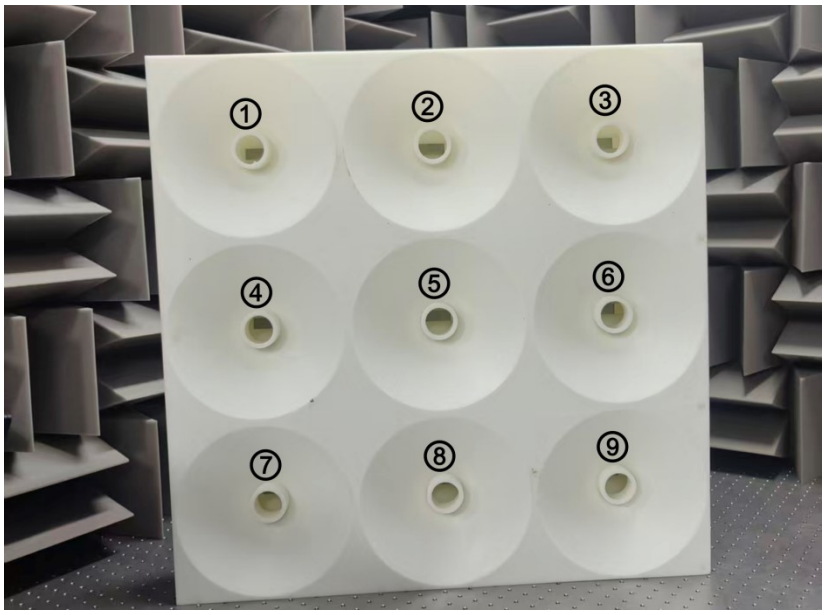

Fig. S8. Meta-surface acoustic barrier.

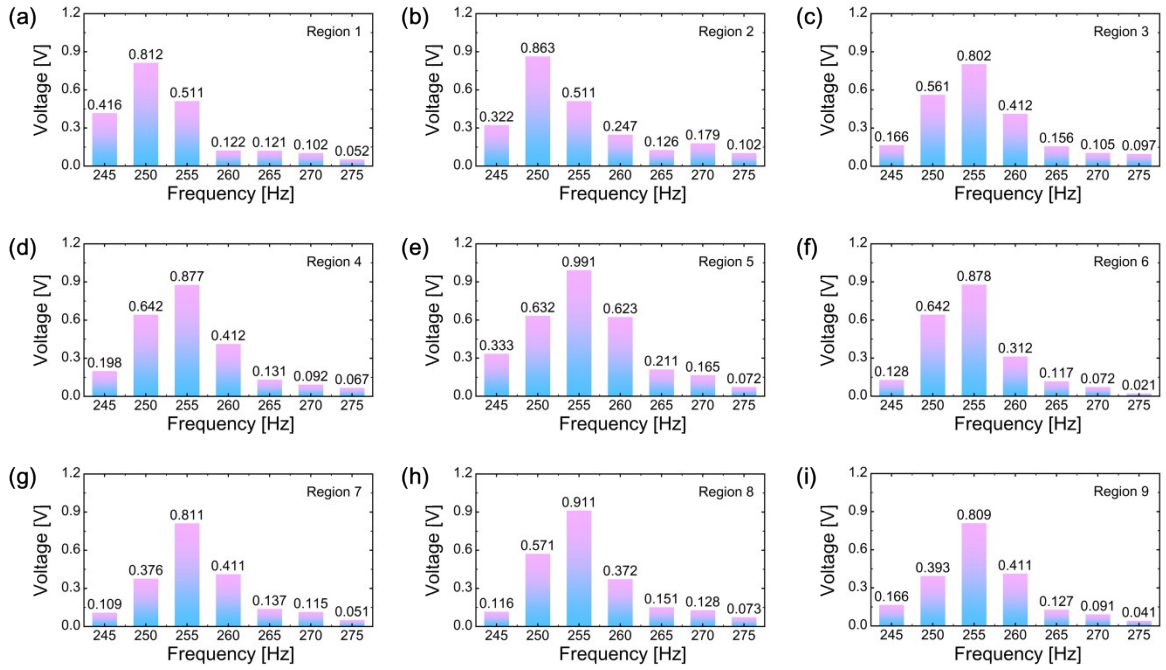

Fig. S9. Energy harvesting performance of the nine regions of the meta-surface acoustic barrier.

References

[1] Y. F. Zhang, J. Li, S. T. Zhu and H. Z. Zhao, *Chaos*, 2023, 33, 083153.

[2] X. Z. Wang, X. F. Kang and Q. G. Lei, *CMES-Comp*. *Model*. *Eng*. *Sci*., 2023, 137, 1749-1771.

[3] V. Alamo Vargas, E. Gourdon, A. Ture Savadkoohi, Nonlinear. Dyn., 2018, 91, 217–231.

[4] X. Q. Ma, H. T. Li, S. X. Zhou, Z. C. Yang, G. Litak, Mech. Syst. Signal. Process., 2022, 168, 108612.